Applications of Magnetohydrodynamics for Heat Transfer Enhancement

Applications of Magnetohydrodynamics for Heat Transfer Enhancement

By

Mehdi Fakour, Davood Domiri Ganji and Alireza Ahmadi

Cambridge Scholars Publishing

Applications of Magnetohydrodynamics for Heat Transfer Enhancement

By Mehdi Fakour, Davood Domiri Ganji and Alireza Ahmadi

This book first published 2023

Cambridge Scholars Publishing

Lady Stephenson Library, Newcastle upon Tyne, NE6 2PA, UK

British Library Cataloguing in Publication Data
A catalogue record for this book is available from the British Library

ISBN (10): 1-5275-1507-9
ISBN (13): 978-1-5275-1507-9

CONTENTS

List of Figures x

List of Tables... xx

Preface xxiii

Chapter 1 1
Magnetohydrodynamics: Definition and Applications
Abstract 1
What is Magnetohydrodynamics? 1
The governing equations 2
MHD in convection 3
Convection of the magnetic field.. 4
Alfvén's Theorem 4
Conclusion... 6
References 6

Chapter 2 7
MHD Forced Convection Heat Transfer
Part 1: Numerical investigation of forced convection heat transfer of Fe3O4-water nanofluid in the presence of an external magnetic source 8
Abstract 8
Introduction 8
Problem statement 10
Governing formulation.. 11
Results and discussion... 21
Conclusions 25
Part 2: Forced convection analysis for MHD Al2O3–water nanofluid flow over a horizontal plate.. 27
Abstract 27
Introduction 27
Description of the problem... 29
Results and discussion... 33
Conclusion... 36

Part 3: Effect of non-uniform magnetic field on forced convection transfer of the heat of Fe3O4–water nanofluid ... 38
Abstract ... 38
Introduction ... 38
Geometry definition and boundary conditions ... 40
Mathematical modeling and numerical procedure ... 41
Problem formulation ... 41
Numerical procedure ... 47
Grid testing and code validation ... 47
Results and discussion ... 48
Conclusions ... 54
Part 4: Numerical investigation of magnetic nanofluid forced convective heat transfer in the existence of variable magnetic field using a two-phase model ... 56
Abstract ... 56
Introduction ... 56
Geometry definition and boundary conditions ... 59
Mathematical modeling and numerical procedure ... 61
Problem formulation ... 61
Numerical procedure ... 69
Grid testing and code validation ... 70
Results and discussion ... 71
Conclusions ... 72
References ... 73

Chapter 3 ... 79
MHD Mixed Convection Heat Transfer
Part 1: Magnetohydrodynamic mixed convective flow of an Al2O3–water nanofluid inside a vertical microtube ... 80
Abstract ... 80
Introduction ... 80
Mathematical modeling ... 83
Results and discussions ... 89
Brownian motion and thermophoresis effects ... 90
Slip and concentration effects ... 92
Magnetic field and mixed convective effects ... 94
Transferring the heart rate and pressure drop ... 96
Conclusions ... 98

Part 2: MHD mixed convection in a vertical annulus filled with Al2O3–water nanofluid considering nanoparticle migration 101
Abstract 101
Introduction 101
Migration of nanoparticles 103
Problem formulation and governing equations........ 105
Boundary conditions 112
Numerical method and accuracy 114
Results and discussions 116
Velocity, temperature, and concentration profiles........ 117
Transferring the heat rate and pressure drop 120
Summary and conclusions 121
Part 3: Nanoparticle transport effect on magnetohydrodynamic mixed convection of electrically conductive nanofluids in micro-annuli with temperature-dependent thermophysical properties 124
Abstract 124
Introduction 124
Problem description and governing equations........ 128
Numerical solution 136
Results and discussion 137
Accuracy of the results........ 138
Velocity, temperature, and concentration profiles........ 139
Transferring the heat enhancement and dropping off the pressure increment 144
Summary and conclusions 147
References 150

Chapter 4 157
MHD Natural Convection Heat Transfer
Part 1: Transportation of MHD nanofluid free convection in a porous semi-annulus using a numerical approach 159
Abstract 159
Introduction 159
Problem definition 161
Governing equation and simulation........ 162
Mesh independent test and verification 172
Results and discussion........ 172
Conclusion........ 173

Part 2: Free convection of magnetic nanofluid considering MFD viscosity effect 175
Abstract 175
Introduction 175
Mathematical modeling and numerical procedure 178
Problem formulation 178
Numerical procedure 185
Grid testing and code validation 185
Results and discussion 186
Conclusions 189
Part 3: MHD free convection in an eccentric semi-annulus filled with nanofluid 191
Abstract 191
Introduction 191
Problem definition and mathematical model 194
Problem statement 194
The lattice Boltzmann method 194
Boundary conditions 197
Curved boundary treatment for temperature 198
The lattice Boltzmann model for nanofluid 199
Grid testing and code validation 200
Results and discussion 202
Conclusions 213
References 215

Chapter 5 220
MHD Heat Transfer in Porous Applications
Part 1: Heat transfer and fluid flow of blood with nanoparticles through porous vessels in a magnetic field: A quasi-one-dimensional analytical approach 221
Abstract 221
Introduction 221
Problem definition 223
Definition of the problem in medical science 228
Results and discussion 228
Conclusions 238
Part 2: Transport of Magnetohydrodynamic nanofluid in a porous media 240
Abstract 240
Introduction 240

Problem definition 240
Results and discussion 248
Conclusions 251
Part 3: Study of the transfer of heat in a nanofluid MHD flow in a channel with permeable walls 252
Abstract 252
Introduction 252
Problem definition 253
Results and discussion 261
Conclusions 268
References 271

List of Figures

Fig. 1.1. Schematic representation of the formation of sunspots................ 5

Fig. 2.1.2. Contours of the (a) magnetic field strength H; (b) magnetic field intensity component in x direction Hx; and (c) magnetic field intensity component in y direction Hy. 14

Fig. 2.1.3. (a) Comparison of the presented work and numerical results by Khanafer et al. for average Nusselt number and Gr = 104, φ = 0.1, Pr = 6.8 (Cu–Water); (b) Comparison of the presented results and Moallemi et al.'s work on the local Nusselt number over the lid wall at Re = 500, Ri = 0.4, and Pr = 1. 15

Fig. 2.1.4. Isotherm (left) and streamline (right) contours for different values of the Hartmann number, Re = 100 and φ = 0.04. 18

Fig.2.1.5. Isotherm (left) and streamline (right) contours for different values of the Hartmann number, Re = 300 and φ = 0.04. 19

Fig. 2.1.6. Isotherm (left) and streamline (right) contours for different values of the Hartmann number, Re = 600 and φ = 0.04. 20

Fig. 2.1.7. Effects of the Hartmann number, the Magnetic number and various Reynolds numbers (a) including Re = 100, (b) Re = 300, and (c) Re = 600 on local Nusselt number Nuloc along the bottom wall. 21

Fig. 2.1.8. Effects of the Hartmann number, Magnetic number and Reynolds number on local and average Nusselt numbers along the bottom wall. 23

Fig. 2.1.9. Effects of the Hartmann number, Magnetic number, and Reynolds number on heat transfer enhancement. 24

Fig. 2.2.1. Schematic of the nanofluid boundary layer on a horizontal plate when there is magnetic field. 30

Fig. 2.2.2. The $\hbar 1$-validity for different orders (15th, 16th and 17th) of approximation (a) Ec = 0.1, m = 0.1, Pr = 6.2, ϕ = 0.05 and Mn = 0.5, (b) Ec = 0.1, m = 0.1, Pr = 6.2, ϕ = 0.05 and Mn = 5. 32

Fig. 2.2.3. The $\hbar 2$-validity for different orders (15th, 16th and 17th) of approximation (a) Ec = 0.1, m = 0.1, Pr = 6.2, ϕ = 0.05 and Mn = 0.5, (b) Ec = 0.1, m = 0.1, Pr = 6.2, ϕ = 0.05 and Mn = 5. 33

Fig. 2.2.4. Comparison of HAM and numerical solution in different Mn numbers when Ec = 0.1, m = 0.1, Pr = 6.2, and ϕ = 0.05 for (a) temperature profile, (b) velocity profile. 35

Fig. 2.2.5. Effect of nanoparticles volume fraction when Ec = 0.1, m = 0.1, Pr = 6.2, and Mn = 0.5 on non-dimensional (a) temperature profile, (b) velocity profile. 35

Fig.2.2.6. Effect of the magnetic parameter (Mn) when Ec = 0.1, m = 0.1, Pr = 6.2, and ϕ = 0.05 on non-dimensional (a) temperature profile, (b) velocity profile. 36

Fig. 2.3.1. (a) Geometry and boundary conditions; (b) The mesh of the enclosure considered in this work; (c) A sample triangular element and its corresponding control volume. 41

Fig. 2.3.2. Contours of the (a) magnetic field strength H; (b) magnetic field intensity component in x direction Hx; (c) magnetic field intensity component in y direction Hy. 42

Fig. 2.3.3. (a) Comparison of average Nusselt number between the present study and the numerical results by Khanafer et al. (2003) Gr = 104, φ = 0.1 and Pr = 6.8 (Cu–Water); (b) Comparison of the local Nusselt number over the lid wall between the present results and Moallemi and Jang (1992) at Re = 500, Ri = 0.4, and Pr = 1. 48

Fig. 2.3.4. Isotherm (left) and streamline (right) contours for different values of Hartmann number when Re = 10. 50

Fig. 2.3.5. Isotherms (left) and streamlines (right) contours for different values of Hartmann number when Re = 100. 51

Fig. 2.3.6. Isotherms (left) and streamlines (right) contours for different values of Hartmann number when Re = 1000. 52

Fig. 2.3.7. Effects of Hartmann and Reynolds numbers on local Nusselt number Nuloc along the hot wall when $\varphi = 0.04$...................................... 53

Fig. 2.3.8. Effects of Hartmann and Reynolds numbers on local Nusselt number Nuave along the hot wall when $\varphi = 0.04$. 53

Fig. 2.3.9. Effects of Reynolds number and Hartmann number on transfer of the heat enhancement. 54

Fig. 2.4.1. (a) Geometry and the boundary conditions; (b) the mesh of enclosure considered in this work; (c) a sample triangular element and its corresponding control volume. 60

Fig. 2.4.2. Contours of the (a) magnetic field strength H; (b) magnetic field intensity component in the x direction Hx; (c) magnetic field intensity component in the y direction Hy. 62

Fig. 2.4.3. (a) Comparison of the local Nusselt number over the lid wall between the present results and Moallemi and Jang at Re = 500, Ri = 0.4, and Pr = 1; (b) Comparison of average Nusselt number between the present results and numerical results by Khanafer et al. Gr = 104, $\phi = 0.1$ and Pr = 6.8(Cu − Water). 63

Fig. 2.4.4. Comparison of the isotherms, streamlines, is concentrations, and heat line contours for different values of Hartmann number when Le = 4, Nt = Nb = 0.5, Re = 10, and Pr = 6.85... 65

Fig. 2.4.5. Comparison of the isotherms, streamlines, is concentrations, and heat line contours for different values of Hartmann number when Le = 4, Nt = Nb = 0.5, Re = 100, and Pr = 6.85... 66

Fig. 2.4.6. Comparison of the isotherms, streamlines, is concentrations, and heat line contours for different values of Hartmann number when Le = 4, Nt = Nb = 0.5, Re = 500, and Pr = 6.85... 67

Fig. 2.4.7. Effects of the Hartmann number, Reynolds number, and Lewis number on the local Nusselt number Nuloc along the hot wall. 69

Fig. 2.4.8. Effects of the Hartmann number, Reynolds number, and Lewis number on the average Nusselt number Nuave along the hot wall........... 70

Fig. 3.1.1. The geometry of the physical model and coordinate system.... 84

Fig. 3.1.2. Comparison of numerical results for NuB = HT C× kbf =kB with those reported by Yang et al. when Ng = λ = Ha = 0. 90

Fig. 3.1.3. The effects of NBT on nanoparticle distribution (ϕ=ϕB), velocity (u/uB), and temperature T/Tn profiles when Ha = 5, Ng = 1, ϕB = 0.06 and λ = 0.1. 91

Fig. 3.1.4. The effects of λ (when ϕB = 0.06) and ϕB (when λ = 0.1) on nanoparticle distribution (ϕ / ϕB), velocity (u/uB) and temperature (T/TB) profiles when Ha = 5, NBT = 1, and Ng = 1... 93

Fig. 3.1.5. The effects of Ha (when Ng = 1) and Ng (when Ha = 5) on nanoparticle distribution (ϕ / ϕB), velocity (u/uB), and temperature (T/TB) profiles when λ = 0.1, NBT = 1, and ϕB = 0.06....................................... 94

Fig. 3.1.6. The effects of λ on the dimensionless heat transfer coefficient HTC (a) and pressure drop (b) when Ha = 5, Ng = 1, and ϕB = 0.06........ 95

Fig. 3.1.7. The effects of Ha on the dimensionless heat transfer coefficient HTC (a) and pressure drop (b) when Ng = 1, ϕB = 0.06, and λ = 0.1. 96

Fig. 3.1.8. The effects of ϕB on the dimensionless heat transfer coefficient HTC (a) and pressure drop(b) when Ng = 1, Ha = 5, and λ = 0.1. 97

Fig. 3.1.9. The effects of ϕB on the dimensionless heat transfer coefficient HTC (a) and pressure drop (b) when ϕB = 0.06, Ha = 5, and λ = 0.1........ 98

Fig. 3.2.1. The geometry of the physical model and coordinate system.. 106

Fig. 3.2.2. Algorithm of the numerical method. 111

Fig. 3.2.3. The effects of NBT (ϕB = 0.06) and ϕB (NBT = 0.5) on nanoparticle distribution (ϕ/ϕB), velocity (u/uB) and temperature (θ/θB) profiles when ε = 0.5, Nr = 50, Ng = 50, Ha = 5 and ζ = 0.6.................. 112

Fig. 3.2.4. The effects of Ng and Nr (Ha = 5) and Ha (Nr = Ng = 50) on nanoparticle distribution ($\phi/\phi B$), velocity (u/uB) and temperature ($\theta/\theta B$) profiles when $\varepsilon = 0.5$, $\phi B = 0.06$, NBT = 0.5 and $\zeta = 0.6$. 113

Fig. 3.2.5. The effects of ζ ($\varepsilon = 0.5$) and ε ($\zeta = 0.06$) on nanoparticle distribution ($\phi/\phi B$), velocity (u/uB) and temperature ($\theta/\theta B$) profiles when $\phi B = 0.06$, Nr = 50, Ng = 50, Ha = 5 and NBT = 0.5. 115

Fig. 3.3.1. The geometry of the physical model and coordinate system: a) longitudinal cross-section and b) transverse cross-section. 126

Fig. 3.3.2. Algorithm of the numerical method. 140

Fig. 3.3.3. The effects of ε on (a) velocity (u / uB), (b) temperature (T*), and nanoparticle distribution (ϕ / ϕB) profiles when $\lambda = 0.01$, $\phi = 0.02$, N = 0.3, Nr = 50 and Ha = 3.0. 141

Fig. 3.3.4. The effects of Ha on (a) velocity (u / uB), (b) temperature (T*), and nanoparticle distribution (ϕ / ϕB) profiles when $\lambda = 0.01$, $\phi = 0.02$, N = 0.3, Nr = 50 and $\varepsilon = 0.5$. 142

Fig. 3.3.5. The effects of λ on (a) velocity (u / uB), (b) temperature (T*), and nanoparticle distribution (ϕ / ϕB) profiles when Ha = 3.0, $\phi = 0.02$, N = 0.3, Nr = 50 and $\varepsilon = 0.5$. 143

Fig. 3.3.6. The effects of Nr on (a) velocity (u / uB), (b) temperature (T*), and nanoparticle distribution (ϕ / ϕB) profiles when Ha = 3.0, $\phi = 0.02$, N = 0.3, $\lambda = 0.01$ and $\varepsilon = 0.5$. 145

Fig. 3.3.7. The effects of ζ on (a) velocity (u / uB), (b) temperature (T*), and nanoparticle distribution (ϕ / ϕB) profiles when $\lambda = 0.01$, $\varepsilon = 0.5$, N = 0.3, Nr = 50 and Ha = 3.0. 146

Fig. 3.3.8. The effects of ε on the heat transfer coefficient ratio (a) and the pressure drop ratio (b) when $\lambda = 0.01$, $\phi = 0.02$, Nr = 50, and Ha = 3.0.. 147

Fig. 3.3.9. The effects of Ha on the heat transfer coefficient ratio (a) and the pressure drop ratio (b) when $\lambda = 0.01$, $\varepsilon = 0.5$, Nr = 50, and $\phi = 0.02$.147

Fig. 3.3.10. The effects of λ on transferring the heat coefficient ratio (a) and the pressure drop ratio (b) when ϕ = 0.02, ε = 0.5, Nr = 50, and Ha = 3.0. 148

Fig. 3.3.11. The effects of Nr on transferring the heat coefficient ratio (a) and the pressure drop ratio (b) when λ = 0.01, ε = 0.5, ϕ = 0.02, and Ha = 3.0. 148

Fig. 3.3.12. The effects of ζ on the heat transfer coefficient ratio (a) and the pressure drop ratio (b) when λ = 0.01, ε = 0.5, Nr = 50, and Ha = 3.0. ... 149

Fig. 4.1.1. (a) Geometry and boundary conditions; (b) the mesh of the geometry considered in this work; (c) a sample triangular element and its corresponding control volume. 162

Fig. 4.1.2. Comparison of the present solution with previous work (Kim et al.) for different Rayleigh numbers when Ra = 103, Pr = 0.7; (b) comparison of the temperature on the axial midline between the present results and numerical results obtained by Khanafer et al. for Gr = 104, ϕ = 0.1 and Pr = 6.2 (Cu – Water). 165

Fig. 4.1.3. Impact of nanofluid volume fraction on streamlines (left) and isotherms (right) contours (nanofluid (ϕ = 0.0.4) (--) and fluid (ϕ = 0) (---) when Ra = 105. 167

Fig. 4.1.4. Isotherms (left) and streamlines (right) contours for different Rayleigh and Hartmann numbers values for porous medium when ϕ = 0.0.4, ξ = 0˚ 167

Fig. 4.1.5. Isotherms (left) and streamlines (right) contours for different Rayleigh and Hartmann numbers values for porous medium when ϕ = 0.0.4, ξ = 90˚ 169

Fig. 4.1.6. Effects of the inclination angle, Rayleigh number, and Hartmann number for porous medium on local Nusselt number at ϕ = 0.0.4. 170

Fig. 4.1.7. Effects of the inclination angle, Rayleigh number, and Hartmann number for porous medium on average Nusselt number. 171

Fig. 4.2.1. (a) Geometry and the boundary conditions; (b) A sample triangular element and its corresponding control volume........................ 176

Fig. 4.2.2. Comparison of average Nusselt number between the present study and the numerical results of Khanafer et al. Gr =104, ϕ=0.1, and Pr = 6.2 (Cu−Water)... 181

Fig. 4.2.3. Effects of viscosity parameter (δ* = 1 (---) and δ* = 0 (--)) and Hartmann number on isotherms (right) and streamlines (left) when ϕ = 0.04, Ra = 103. 182

Fig. 4.2.4. Effects of viscosity parameter (δ* = 1 (---) and δ* = 0 (--)) and Hartmann number on isotherms (right) and streamlines (left) when ϕ = 0.04, Ra = 104. 185

Fig. 4.2.6. Effects of Hartmann and Rayleigh numbers on local Nusselt numbers when ϕ = 0.04, δ* = 1, Pr = 6.2... 187

Fig. 4.2.7. Effects of Hartmann and Rayleigh numbers on average Nusselt numbers when ϕ = 0.04, δ = 1, Pr = 6.2... 188

Fig. 4.2.8. Effects of Hartmann and Rayleigh numbers on Nusselt ratio when ϕ = 0.04, Pr =6.2. 189

Fig. 4.3.1. (a) Discrete velocity set of two-dimensional nine-velocity (D2Q9) model; (b) curved boundary and lattice nodes............................ 196

Fig. 4.3.2. Comparison of isotherms between the present work and experimental study of (a) Kuehn and Goldstein; and (b) Laboni and Guj for viscous flow (ϕ = 0, Pr = 0.7) when (a) R0 / Ri = 2.6, Ra = 4.7×104; (b) R0 = Ri = 2.36, Ra = 0:9×105.. 201

Fig. 4.3.4. Comparison of the isotherms (left) and streamlines (right) contours between nanofluid (ϕ = 0.06) (--) and pure fluid (ϕ = 0) (---) for different values of Ha and δ/L at λ = 3.5; Ra = 106 and Pr = 6.8. 205

Fig. 4.3.5. Effects of Ha, Ra, and d=L on isotherms (left) and streamlines (right) contours for Cu-water case (ϕ = 0.06) when λ = 3.5 and Pr = 6.8.206

Fig. 4.3.6. Effects of Ha, Ra, δ/L, and ϕ on local Nusselt number along the enclosure (Nuc) walls for Cu-water case when λ = 3.5 and Pr = 6.8....... 209

Fig. 4.3.7. Effects of Ha, Ra, d=L, and f on local Nusselt number along the inner cylinder (Nuh) surface for Cu-water case when λ = 3.5 and Pr = 6.8... 210

Fig. 4.3.8. Effects of Ha, Ra, and δ/L on average Nusselt number along (a) the walls of the enclosure (Nuc); (b) the surface of the inner cylinder (Nuh) for Cu-water case when ϕ = 0.06, λ = 3.5. 211

Fig. 4.3.9. Variation of average Nusselt number along (a) the walls of the enclosure (Nuc), (b) the surface of the inner cylinder (Nuh) for various input parameters. 212

Fig. 4.3.10. Effects of Ha, Ra, and δ/L on the ratio of enhancement in heat transfer due to the addition of nanoparticles for Cu-water case when λ = 3.5. 213

Fig. 4.3.11. Effects of types of nanoparticles on enhancement in heat transfer due to addition of nanoparticles when λ = 3.5, Pr = 6:8, Ha = 0. 213

Fig. 5.1.1. Schematic of blood flow through a porous artery in a magnetic field.. 224

Fig. 5.1.2. Comparison of HPM with NUM for θ, ϕ, V when Nb = Nt = α = ʌ = P = M = C = Gr = Br =1, μ(r) = 1.. 230

Fig. 5.1.3. Effect of pressure gradient on the velocity profile. 231

Fig. 5.1.4. Effect of porosity parameter on the velocity profile.............. 232

Fig. 5.1.5. Effect of thermophoresis parameter on the velocity profile. .. 232

Fig. 5.1.6. Effect of Brownian motion parameter on the velocity profile.233

Fig. 5.1.7. Effect of thermophoresis parameter on the temperature profile. 234

Fig. 5.1.8. Effect of Brownian motion parameter on the temperature profile. 234

Fig. 5.1.9. Effect of thermophoresis parameter on nanoparticles concentration profile... 235

Fig. 5.1.10. Effect of Brownian motion parameter on nanoparticles concentration profile. 236

Fig. 5.1.11. Effect of third-grade parameter on the velocity profile. 236

Fig. 5.1.12. Effect of MHD parameter on the velocity profile. 237

Fig. 5.1.13. Effect of Grashof number on the velocity profile. 237

Fig. 5.1.14. Comparison of various viscosity models for V when Nb = Nt = α = ʌ = P = M = C = Gr = Br =1 239

Fig. 5.2.1. (a) Geometry and the boundary conditions with (b) the mesh of enclosure considered in this work; (c) A sample triangular element and its corresponding control volume. 241

Fig. 5.2.2. Comparison of isotherms between the present work and experimental study of (a) Kuehn and Goldstein; (b) Comparison of the temperature on the axial midline between the present study and the numerical results obtained by Khanafer et al. for Gr = 104, ϕ = 0.1 and Pr = 6.2 (Cu − Water) 243

Fig. 5.2.3. Isotherms (left) and streamlines (right) contours for different values of Rayleigh number and Hartmann number for porous medium when ε = 0.9, ϕ = 0.04, and a = 0.8 245

Fig. 5.2.4. Isotherms (left) and streamlines (right) contours for different values of Rayleigh number and Hartmann number for porous medium when ε = 0.7, ϕ = 0.04, and a = 0.8 247

Fig. 5.2.5. Isotherms (left) and streamlines (right) contours for different values of Rayleigh number and Hartmann number for porous medium when ε = 0.9, ϕ = 0.04, and a = 0.6 248

Fig. 5.2.6. Effects of ε, a, Ra, and Ha for porous medium on average Nusselt number when ϕ = 0.04. 250

Fig. 5.2.7. Effects of Ra and Ha for porous medium on the ratio of heat transfer enhancement due to the addition of nanoparticles when ε = 0.9, a = 0.8. 251

Fig. 5.3.1. Three-dimensional Schematic of the problem. 254

Fig. 5.3.2. Schematic of the problem (nanofluid in a porous Channel and magnetic field). 254

Fig. 5.3.3. Comparison of LSM and numerical results for dimensionless velocities and temperature (a) U(y), (b) V(y), and (c) θ(y). 262

Fig. 5.3.4. The effects of the nanoparticle and liquid phase material on velocity and temperature profiles when Re = Ha = Pr = Ec = 1, φ = 0.04.. 263

Fig. 5.3.5. Effect of nanoparticle volume fraction, φ, on U(y), V(y), and θ(y), for water with copper nanoparticles, when Re = Ha = Pr = Ec= 1.. 264

Fig. 5.3.6. Effect of Hartmann number (Ha) on dimensionless velocities and temperature for water with copper nanoparticles, φ = 0.04, a) V(y), Re = 1, b) U(y), Re = 1, c) θ(y), Re = Pr = Ec = 1, d) V(y), Re = 5, e) U(y), Re = 5, f) θ(y), Re = Pr = Ec = 5. 266

Fig. 5.3.7. Effect of Hartmann number (Ha) on dimensionless velocities and temperature for water with copper nanoparticles, φ = 0.04, a) V(y), Re = 1, b) U(y), Re = 1, c) θ(y), Re = Pr = Ec = 1, d) V(y), Re = 5, e) U(y), Re = 5, f) θ(y), Re = Pr = Ec = 5. 267

Fig. 5.3.8. Effect of Prandtl number on dimensionless temperature for water with copper nanoparticles, φ = 0.04, a) θ(y), Ha = Re = Ec = 1, b) θ(y), Ha = Re = Ec = 10... 268

Fig. 5.3.9. Effect of Eckert number on dimensionless temperature for water with copper nanoparticles, φ = 0.04, a) θ(y), Ha = Re = Pr = 1, b) θ(y), Ha = Re = Pr = 10. 269

Fig. 5.3.10. Velocity and temperature profiles for the different models for Re = Ha = Pr = Ec = 1 and Cu–water case (φ = 0.04). 270

LIST OF TABLES

Table 2.1.1. Thermophysical properties of water and nanoparticles. 15

Table 2.1.2. Comparison of the average Nusselt number Nu_{ave} and the lid wall for different grid resolutions at Re = 600, φ = 0.04, Ha = 40, Ec = $10^{-5,}$ and Pr = 6.8. 15

Table 2.2.1. Physical properties of fluid (Water) and nanoparticles (Aluminum Oxide). 34

Table 2.3.1. Thermophysical properties of water and nanoparticles. 45

Table 2.3.2. Comparison of the average Nusselt number Nu_{ave} along the hot wall for different grid resolutions at Re = 1000, φ = 0.04, H a = 20, E c = 10^{-5}, ε1 = 0, and Pr = 6.8. 48

Table 2.4.1. Comparison of the average Nusselt number Nuave along the hot wall for different grid resolutions at Re = 500, Ha = 20, Le = 4, Ec = 10−5, ε1 = 0, and Pr = 6.8. 63

Table 3.1.1. Results of the numerical solution when λ = 0, Ha = 5, Ng = 1, and ϕ_B = 0:06. 88

Table 3.1.2. Grid independence test for different values of ϕ_B when Ha = 5, Ng = 1, N_{BT} = 1, and λ = 0.1. 89

Table 3.2.1. Validation of the results with the ones reported by Kays and Crawford [69] when $Ha = Nr = Ng = \phi_B = 0$. 109

Table 3.2.2. Comparison of Nu_B with the reported data of Yang et al. when $Nr = Ha = \gamma = Ng = 0, \phi B = 0.02$. 109

Table 3.2.3. Grid independence test for different values of dη when $Ha = 0, N_{BT} = 1, \phi B = 0.02, \varepsilon = 0.5, \zeta = 0.4$, and $Nr = Ng = 50$. 110

Table 3.3.2. Result of the numerical solution when Nr = 150, Ha = 20, λ = 0.01, ζ = 0.5 and ε = 0.5 in the case of without temperature 137

Table 3.3.3. Comparison of numerical results for $HTC \times k_{bf}/k_B$ with the ones reported by Yang et al. when $Nr = Ha = \lambda = 0$ and $\phi_B = 0.02$.......... 137

Table 3.3.4. Compare numerical results for HTC at both walls with those reported by Kays and Crawford when $Nr = \lambda = \phi = Ha = 0$.................. 138

Table 3.3.5. Grid independence test for different values of dη when $N_{BT} = 0.3$, $Ha = 20$, $\lambda = 0.01$, $\varepsilon = 0.5$, $\phi_B = 0.02$, and $Nr = 150$ in the case of without temperature dependency. 138

Table 4.1.1. The coefficient values of CuO - Water nanofluid. 161

Table 4.1.2. Thermophysical properties of water and nanoparticles. 163

Table 4.1.3. Comparison of Nu_{ave} for different grid resolutions at $Ra = 10^3$, $\xi = 90^\circ$, $Ha = 20$, and $\phi = 0.04$. 163

Table 4.1.4. Average Nusselt number versus different Grashof numbers under various strengths of the magnetic field at $Pr = 0.733$. 166

Table 4.1.5. Effects of ξ, Ha, and Ra on heat transfer enhancement. 173

Table 4.2.1. The coefficient values of Al2O3 - Water nanofluid. 177

Table 4.2.2. Thermophysical properties of water and nanoparticles. 178

Table 4.2.3. Comparison of Nu_{ave} for different grid resolutions at $Ra = 10^5$, $\delta^* = 1$, $Ha = 60$ and $\phi = 0.04$, $Pr = 6.2$. 180

Table 4.2.4. Average Nusselt number versus different Grashof numbers under various strengths of the magnetic field at $Pr = 0.733$. 180

Table 4.3.1. Thermo physical properties of water and nanoparticles. 199

Table 4.3.2. Comparison of the average Nusselt number along the surface of the inner cylinder for different grid resolutions at $Ra = 10^5$, $\delta/L = 0.8$, $Ha = 40$, and $\phi = 0.06$. 201

Table 4.3.3. Average Nusselt number versus different Grashof numbers under various strengths of the magnetic field at $Pr = 0.733$. 203

Table 4.3.4. The constant coefficient for using Eq. (4.3.23). 207

Table 4.3.5. The constant coefficient for using Eq. (4.3.24). 208

Table 5.1.1. Comparison of HPM with NUM for θ, ϕ, V when $Nb = Nt = \alpha = \lambda = P = M = C = Gr = Br = 1$, $\mu(r) = 1$ 229

Table 5.1.2. The errors of HPM for θ, ϕ, V when $Nb = Nt = \alpha = \lambda = P = M = C = Gr = Br = 1$, $\mu(r) = 1$ 231

Table 5.3.1. Different models for simulation of Dynamic viscosity........ 257

Table 5.3.2. Thermophysical properties of nanofluids and nanoparticles.258

PREFACE

Magnetohydrodynamics (MHD) can be defined as the study of magnetic properties and the behavior of electrically conducting fluids. These sorts of magneto-fluids include, for instance, plasmas, liquid metals, salt water, and electrolytes. The term "Magnetohydrodynamics" derives from the words “magneto” (meaning magnetic field), “hydro” (meaning water), and “dynamics” (as in movement). The underlying basis of MHD can be explained in layman’s terms as follows: currents in moving conductive fluids and magnetic fields can lead to induction currents, making the fluid polarized. This can also alter the magnetic field itself reciprocally. To describe MHD, Navier–Stokes equations of fluid dynamics are combined with Maxwell’s equations of electro-magnetism. We must solve all of them simultaneously, using analytical or numerical methods.

We can define nanofluids as fluids that include particles that are nanometers in size. These fluids can be engineered to become colloidal suspensions of nanoparticles in a base fluid. The nanoparticles used in nanofluids are typically made of metals, oxides, carbides, or carbon nanotubes. Common base fluids include water, ethylene glycol, etc. Nanofluids have novel properties that make them potentially useful for transferring heat, for instance through microelectronics, fuel cells, pharmaceutical processes, hybrid-powered engines, engine cooling/vehicle thermal management, domestic refrigerators, chillers, heat exchangers, grinding, machining, and boiler flue gas temperature reduction. Through the use of nanofluids, the heat transfer coefficient and thermal conductivity would be higher compared to the base fluid.

The first chapter of this book examines the definition and applications of magnetohydrodynamics (MHD), including MHD in heat conduction. In the second chapter, the MHD forced convection transfer of the heat is carried out. Here we try to study the forced convective transfer of the heat from various nanofluids' applications numerically. The third chapter examines the MHD mixed convective flow of nanofluids inside the microchannel and other applications. Finally, the transportation of MHD nanofluid free convection in different applications is studied in the last chapter.

Numerical and analytical methods are applied to solve the governing nonlinear differential equations of the problems discussed. The book also attempts to demonstrate the reliability and accuracy of these methods. Furthermore, the impact of some physical parameters and dimensionless numbers on the flow, velocity, and temperature profiles of nanofluids is scrutinized.

CHAPTER 1

MAGNETOHYDRODYNAMICS: DEFINITION AND APPLICATIONS

Abstract

Magnetohydrodynamics (MHD) can be defined as the study of the dynamics of electrically conducting fluids. Magnetohydrodynamics creates a relationship between the Navier-Stokes equations for fluid dynamics and Maxwell's equations for electromagnetism. The fundamental basis of Magnetohydrodynamics is that magnetic fields in a conducting and moving fluid can lead to the induction of currents which create forces on the fluid, and which in turn can influence the magnetic field. This chapter defines Magnetohydrodynamics and the governing equations for MHD in convection heat transfer.

What is Magnetohydrodynamics?

The considerable influence magnetic fields exert on fluids and flows is something that we can all see in both nature and artificial processes. Magnetic fields can be used for stirring, pumping, levitating, and heating liquid metals in the metallurgical industry. Even the earth's magnetic field, which protects the surface of our planet from harmful radiation, is generated by the motion of the earth's core, which is liquid. Furthermore, the sun's rotating magnetic fields create sunspots and solar flares (sudden explosions of energy) and galactic magnetic fields affect the formation of stars from interstellar gas clouds. Henceforth, the word Magnetohydrodynamics (MHD) is used for all of these phenomena. Here, the magnetic field, which is denoted as *B,* can be coupled with the velocity field, shown as U, under the condition that a conducting, non-magnetic fluid such as a liquid metal, a hot ionized gas (plasma) or a strong electrolyte is applied. The complex interaction between the currents generated by the magnetic field and the moving fluid causes forces to act on the fluid itself, resulting in the magnetic field alteration.

The governing equations

The main aim of this section is to extract the governing equations of MHD based on the information provided. First of all, we will consider a non-magnetic fluid that is conducting and Newtonian, and has uniform kinematic viscosity (fluids with a v = const., and incompressible flow). We use the following equations based on the works of Davidson (2001) and Moreau (1990) as the reduced Maxwell's equations:

$$\nabla \times B = \mu J, \qquad \nabla . J = 0 \tag{1.1}$$

$$\nabla \times E = -\frac{\partial B}{\partial t}, \qquad \nabla . B = 0 \tag{1.2}$$

With Ohm's law and the Laplace force:

$$J = \sigma\left(E + u \times B\right), \qquad F = J \times B \tag{1.3}$$

Combining the above equations, we derive a transportation equation for **B**

$$\frac{\partial B}{\partial t} = \nabla \times \left(u \times B\right) + \lambda \Delta B \tag{1.4}$$

where $\lambda = (\sigma\mu)^{-1}$ is the magnetic diffusivity.

On the other hand, the Navier-Stokes equations for incompressible flow can be derived from the motion equations as follows:

$$\frac{\partial u}{\partial t} + \left(u . \nabla\right) - \upsilon \Delta u + \frac{1}{\rho}\nabla p = \frac{1}{\rho} f, \qquad \nabla . u = 0 \tag{1.5}$$

Substituting the Lorentz force (1.3) for f, we have:

$$\frac{\partial u}{\partial t} + \left(u . \nabla\right) - \upsilon \Delta u + \frac{1}{\rho}\nabla p = \frac{1}{\rho} J \times B, \qquad \nabla . u = 0 \tag{1.6}$$

where $v = \mu_f / \rho$ is the kinematic viscosity.

To determine MHD, another form of the Navier-Stokes equations can be introduced. Let $\omega = \nabla \times u$ denote the vorticity field. Using the vector identity $\nabla(u^2/2) = (u \cdot \nabla)\, u + u \times (\nabla \times u)$ and neglecting the other forces f, we can restate the first equation as:

$$\frac{\partial u}{\partial t} + \nabla\left(u^2/2\right) - u \times \omega - \upsilon \Delta u + \frac{1}{\rho} \nabla p = 0 \tag{1.7}$$

Since the curl of a gradient of a scalar function is zero, we can switch the order of the differential operators and take the curl of Eq. (1.7) to simplify it in the following form:

$$\frac{\partial \omega}{\partial t} = \nabla\left(u \times \omega\right) + \upsilon \Delta u \tag{1.8}$$

Eq. (1.8) is defined as the vorticity equation.

MHD in convection

Thus far, we have created a coupling between electromagnetism and fluid dynamics equations. The rest of this chapter is devoted to further examining half of the coupling. For practical applications, we neglect the NSE and take the velocity field u as prescribed. It is of great importance to mention that comparing Eqs. (1.4) and (1.8) is totally incorrect and does not produce reliable results since the relationship between u and ω is completely different than that of u and B. Due to the same differential operators existing in the governing equations, we have analogous results for MHD and classical vortex dynamics.

For the induction equation, consider $\nabla \cdot u = 0$ and use equation $\nabla \times (u \times B) = (B \cdot \nabla)u - (u \cdot \nabla)B$, which leads to the following expression:

$$\frac{\partial B}{\partial t} + \left(u . \nabla\right) B = \left(B . \nabla\right) u + \lambda \Delta B \tag{1.9}$$

The terms on the left side of the above equation show the total derivative of B, denoted by D_B / D_t. (u · ∇)B, that represents the changes occurring in the magnetic field. These changes are created by fluid particles that enter or leave a tiny volume. If the velocity field u is parallel to the direction of the greatest change in *B*, it can be considered important. In Eq. (1.8), the creation process of the field can be seen on the first side of the equation. It is shown by stretching the field lines. If the flow and the magnetic field are perpendicular to each other, then it is zero, but near the stagnation points, this term is maximized. Diffusion of the magnetic field can be shown in the second term of the right side of Eq. (1.9), which demonstrates the transportation of the magnetic field via diffusion observed in different phenomena, such as heat.

Convection of the magnetic field

Here, λ is considered to be so small that it can be neglected (λ ≈ 0). In this case, there is no diffusion, so the induction equation is introduced as follows:

$$\frac{\partial B}{\partial t} = \nabla \times \left(u \times B \right) \tag{1.10}$$

This is identical to the vorticity equation for inviscid fluids. Therefore, two important results of Vortex theory - Helmholtz's first law of thermodynamics and Kelvin's theorem - have their analogies in MHD and can be merged to form Alfvén's theorem.

Alfvén's Theorem

1. The fluid elements lying on a magnetic field line at some initial instant continue to lie on that line for all time, i.e., the field lines are frozen into the fluid.

2. The magnetic flux that links any loop moving with the fluid is constant. In other words:

$$\frac{d}{dt}\int_{S(t)} B \,.\vec{n}\, ds = 0 \tag{1.11}$$

S(t) denotes a surface bounded by a closed curve *C(t)*. To satisfy λ = 0, we need large magnetic Reynolds numbers. Of course, in astrophysics, the magnetic Reynolds numbers can exceed values of ~ 108 because of the enormous length scales that usually happen. Sunspots are an excellent example of the frozen-in behavior of magnetic field lines in astrophysics.

To understand their mechanics, we must study the structure of the sun. In the first place, we must consider its surface: the sun's surface is not uniformly bright and it has a granular structure due to the convective turbulence on its outer layer.

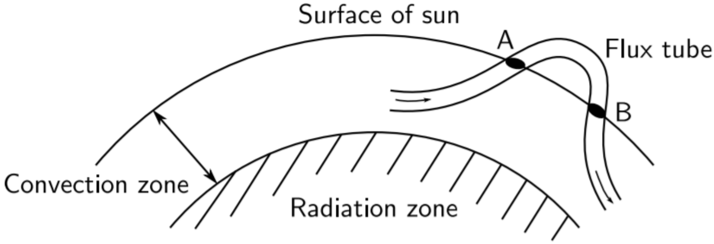

Fig. 1.1. Schematic representation of the formation of sunspots

The outer layer, called the convective layer, has an average thickness of 2∗105 [km]. This layer consists of convection cells, constituting a pattern that is evolving gradually. When the hotter and brighter cells rise to the surface, colder and darker cells sink back into the interior, forming the granular pattern of the sun's surface. This happens with a velocity of almost 1[km/s], which leads to an estimate of the (magnetic) Reynolds numbers, i.e., Re $\sim 10^{11}$ and Rem $\sim 10^{8}$, that are very large. The average magnetic field of the sun is also a few Gauss [Gs], which is very near to the earth's one (1[Gs] = 10^{-4} [T] = 10^{-4} [V s/m2]). Due to the highly magnetic Reynolds number, the magnetic field likely freezes in the fluid. As a result of the existing differential rotation, the magnetic field is stretched and intensified, and ultimately this causes the field strength to rise in horizontal flux tubes. Considering the Lorentz force points radially outward from these tubes, the pressure and density inside these tubes are less than the pressure and density of the surroundings, leading to a buoyancy force. When the thickness of the tubes is very thick, this force is so strong that it can partially destabilize the convection, so these parts tend to drift towards the surface. It has been seen that occasionally flux tubes with a diameter of $\sim 10^{4}$ [km] emerge through the surface into the sun's atmosphere. Sunspots are the areas inside of which the flux tube leaves and re-enters the surface of the sun (A and B in Fig. 1.1). The magnetic field in the flux tubes has a very high field strength (~ 3000[Gs]), so it can cool the surface in these areas by suppressing fluid motion and convection.

Conclusion

Magnetohydrodynamics studies the dynamics of electrically conducting fluids and relates the Navier-Stokes equations for fluid dynamics and Maxwell's equations for electromagnetism to each other. The main point in this chapter is that the influence of magnetic fields on conductive fluids leads to fluid motion which causes force induction on the fluid that can affect the magnetic field. This chapter introduces the fundamentals of Magnetohydrodynamics, including the governing equations for MHD in convection heat transfer.

References

Davidson P. A. 2001. An introduction to magnetohydrodynamics. Cambridge texts in applied mathematics. Cambridge Univ. Press, Cambridge.

Engl H. W., Neubauer A. 2012. Skriptum Analysis. Institut für Industriemathematik, Johannes Kepler Universität Linz.

Fleisch D. A. 2011. A student's guide to Maxwell's equations. Cambridge Univ. Press, Cambridge.

Griffiths D. J. 2008. Introduction to electrodynamics. Pearson, Benjamin Cummings, San Francisco, Calif.

Langer. U. 2014. Lecture notes on Mathematical Methods in Engineering. Institut für Numerische Mathematik, Johannes Kepler Universität Linz.

Moreau R. J. 1990. Magnetohydrodynamics. Fluid mechanics and its applications. 3. Kluwer, Dordrecht. Aus dem Franz. übers.